Whole-Body Imaging of High-Dose Ionizing Irradiation-Induced Tissue Injuries Using ^{99m}Tc-Duramycin

Steven E. Johnson*[1], Zhixin Li*[2], Yu Liu[2], John E. Moulder[3], and Ming Zhao[1]

[1]*Department of Medicine, Feinberg School of Medicine, Northwestern University, Chicago, Illinois;* [2]*Department of Biophysics, Medical College of Wisconsin, Milwaukee, Wisconsin; and* [3]*Department of Radiation Oncology, Medical College of Wisconsin, Milwaukee, Wisconsin*

High-dose ionizing irradiation can cause extensive injuries in susceptible tissues. A noninvasive imaging technique that detects a surrogate marker of apoptosis may help characterize the dynamics of radiation-induced tissue damage. The goal of this study was to prove the concept of imaging the temporal and spatial distribution of damage in susceptible tissues after high-dose radiation exposure, using ^{99m}Tc-duramycin as a phosphatidylethanolamine-binding radiopharmaceutical. **Methods:** Rats were subjected to 15 Gy of total-body irradiation with x-rays. Planar whole-body ^{99m}Tc-duramycin scanning (n = 4 per time point) was conducted at 24, 48, and 72 h using a clinical γ-camera. On the basis of findings from planar imaging, preclinical SPECT data were acquired on control rats and on irradiated rats at 6 and 24 h after irradiation (n = 4 per time point). Imaging data were validated by γ-counting and histology, using harvested tissues in parallel groups of animals (n = 4). **Results:** Prominent focal uptake was detected in the thymus as early as 6 h after irradiation, followed by a gradual decline in ^{99m}Tc-duramycin binding accompanied by extensive thymic atrophy. Early (6–24 h) radioactivity uptake in the gastrointestinal region was detected. Significant signal was seen in major bones in a slightly delayed fashion, at 24 h, which persisted for at least 2 d. This finding was paralleled by an elevation in signal intensity in the kidneys, spleen, and liver. The imaging results were consistent with ex vivo γ-counting results and histology. Relatively high levels of apoptosis were detected from histology in the thymus, guts, and bones, with the thymus undergoing substantial atrophy. **Conclusion:** As a proof of principle, this study demonstrated a noninvasive imaging technique that allows characterization of the temporal and spatial dynamics of injuries in susceptible tissues during the acute phase after high-dose ionizing irradiation. Such an imaging capability will potentially be useful for global, whole-body, assessment of tissue damage after radiation exposure. These data, in turn, will contribute to our general knowledge of tissue susceptibility to ionizing irradiation, as well as the onset and progression of tissue injuries.

Key Words: ^{99m}Tc-Duramycin; phosphatidylethanolamine; apoptosis; radiation injuries

J Nucl Med 2013; 54:1397–1403
DOI: 10.2967/jnumed.112.112490

Received Aug. 8, 2012; revision accepted Feb. 19, 2013.
For correspondence or reprints contact: Ming Zhao, Department of Medicine, Feinberg School of Medicine, Northwestern University, 303 E. Chicago Ave., Chicago, IL, 60611.
E-mail: m-zhao@northwestern.edu
*Contributed equally to this work.
Published online Jun. 26, 2013.

Exposure to high-dose ionizing irradiation, such as in radiation therapy or incidental radiation exposure, can cause injuries in susceptible tissues. There is extensive and growing literature on the temporal and spatial characterization of ionizing irradiation–induced tissue injuries. However, current knowledge is based largely on symptomatic interpretations, functional changes, pathologic and histologic analysis, and in vitro cell-based studies. A noninvasive imaging technique would provide a new approach for dynamic, whole-body assessment of radiation-induced pathophysiologic changes. The availability of a noninvasive imaging technique would contribute to our general knowledge on radiation-induced tissue injuries on a system level. Additionally, this technique might help in the early detection of injury, as well as in monitoring progression of tissue damage and the efficacy of interventional treatments.

Apoptosis is abundant in susceptible tissues after high-dose ionizing irradiation (*1–7*). On a cellular level, the primary cause of cellular injury by ionizing irradiation includes DNA damage, in which severely damaged cells commit to apoptosis (*6,7*). Ionizing irradiation also results in the generation of reactive free-radical species, which attack vital cellular components and can cause cell death (*6,7*). Given that the peak of the early wave of apoptosis arrives within hours after irradiation, apoptotic cell death is one of the earliest manifestations of tissue injury. Detection of radiation-induced apoptosis, therefore, has significant potential in the characterization of tissue injuries in the acute phase.

The externalization of certain phospholipids, such as phosphatidylserine (PS) and phosphatidylethanolamine (PE), is an established molecular marker for apoptosis (*8–11*). In a typical viable mammalian cell, PS and PE are predominantly distributed in the inner leaflet of the plasma membrane in an energy-dependent manner (*9*). During apoptosis, the redistribution of these phospholipids across the bilayer is facilitated. As a result, PS and PE become exposed onto the cell surface (*8–11*). Being major phospholipid components of the plasma membrane, exposed PS and PE provide well-defined molecular targets for detection using phospholipid-targeted imaging agents (*12–14*).

Noninvasive imaging in a whole-body fashion demands that an imaging agent bind avidly to target tissues, with fast systemic clearance and a low general background level. In terms of apoptosis imaging, considerable effort has been invested in developing agents with optimal in vivo binding, biodistribution, and clearance profiles. To this end, ^{99m}Tc-labeled duramycin has been shown to have favorable imaging properties, including high-affinity and high-specificity binding to PE, fast blood clearance, and

a low general background level (*14*). These properties of ^{99m}Tc-duramycin have been studied in depth with quantitative analysis and shown as advantageous over larger, protein-based imaging agents (*14,15*). The combination of these characteristics makes it appropriate to test ^{99m}Tc-duramycin in a whole-body imaging survey. The goal of the current study was to investigate the feasibility of using ^{99m}Tc-duramycin to capture the global dynamics of early cell death induced by high-dose ionizing radiation.

MATERIALS AND METHODS

Total-Body Irradiation

The animal protocol was approved by the Institutional Animal Care and Use Committee under the National Institutes of Health guideline. Barrier-maintained animals (female rats, strain WAG/RijCmcr, 8–10 wk of age with a body weight between 120 and 140 g) underwent total-body irradiation, including the tail. Irradiation was performed on unanesthetized animals placed in a customized jig ($19 \times 3.9 \times 4$ cm) that prevents movement of the rat or its appendages during the irradiation process. The rats were placed in the jig 5–10 min before the irradiation for acclimation, and the irradiation time ranged from 3 to 5 min at 15 Gy of total-body irradiation. The irradiation was delivered in single doses by an orthovoltage x-ray machine. Irradiated rats and age-matched controls were housed under identical conditions until the completion of the study.

Animals

For planar imaging, 4 animals per group were imaged at 1 h after ^{99m}Tc-duramycin injection, and the groups included a control (nonirradiated) group and 24-, 48-, and 72-h postirradiation groups. ^{99m}Tc-methyldiphosphonate (^{99m}Tc-MDP) bone scanning was performed on 4 animals at 24 h after irradiation. For SPECT studies, 4 animals per group were scanned at 1 h after ^{99m}Tc-duramycin injection, and the groups included a control group and 6- and 24-h postirradiation groups. Separate groups of animals were used for tissue analysis. The groups for tissue analysis were a control group and 6-, 24-, 48-, and 72-h postirradiation groups. Four animals per group were injected intravenously with ^{99m}Tc-duramycin and were sacrificed at 1 h after injection. Organs and tissues were collected for γ-counting and histology.

Radiopharmaceutical Preparation

The duramycin was radiolabeled as previously described (*14–17*). More specifically, duramycin was covalently modified by reaction with succinimidyl 6-hydrazinonicotinate acetone hydrazone (HYNIC). One microgram of monoconjugated HYNIC-duramycin was labeled using approximately 74 MBq of ^{99m}Tc-pertechnetate in a single-step kit formulation with the presence of tricine, trisodium triphenylphosphine-3,3′,3″-trisulfonate, and stannous chloride. The reaction vial was heated to 80°C for 20 min before being cooled to room temperature for injection. The radiopharmaceutical was consistently of at least 92% radiochemical purity and was injection-ready according to high-performance liquid chromatography analysis.

In Vivo Studies

For in vivo radionuclide imaging, 2-dimensional planar and 3-dimensional tomographic imaging data were acquired using a clinical γ-camera and a preclinical SPECT scanner, respectively. The use of in vivo imaging was intended to demonstrate the feasibility of detecting radiation-induced tissue injuries in a qualitative fashion. The in vivo imaging results were validated in terms of percentage injected dose per gram (%ID/g) in specific organs and tissues by γ-counting. For anterior whole-body planar imaging, the anesthetized animal was immobilized on the surface of a clinical XRT γ-camera (GE Healthcare) equipped with a low-energy, high-resolution parallel-hole collimator. Static images were acquired at 60 min after ^{99m}Tc-duramycin injection (intravenous, 37 MBq) with 1 million counts, a 22.5×22.5 cm field of view, and an energy window of 140 ± 15 keV. ^{99m}Tc-MDP bone scanning was performed at 24 h after irradiation to examine potential changes in osteogenic activity, with 37 MBq being injected intravenously into 4 animals and whole-body anterior planar images acquired at 30 min after injection. SPECT and CT anatomic data were acquired on a Triumph small-animal SPECT/CT scanner (GE Healthcare) equipped with a quad-detector SPECT system and multipinhole collimators at 1.2-mm spatial resolution. Each animal was injected with ^{99m}Tc-duramycin at approximately 37 MBq of radioactivity via the tail vein. At 60 min after injection, helical SPECT was acquired at an energy window of 140 ± 15 keV with 72 projections at 10 s each, followed by anatomic CT at an energy level of 80 keV. SPECT and CT data were reconstructed and coregistered using inbuilt software.

Tissue Analysis

Results from whole-body radionuclide imaging were validated by γ-counting using dissected tissues. More specifically, control and irradiated animals at 6, 24, 48, and 72 h were sacrificed at 1 h after intravenous injection of ^{99m}Tc-duramycin (3.7 MBq). Different tissues and organs were excised, weighed, and measured in a well counter. The tissues analyzed for γ-counting were the bone, brain, fat, heart, kidneys, liver, lung, muscle, pancreas, skin, small intestine, spleen, stomach, thymus, and thyroids. The amount of radioactivity in each tissue was measured by γ-counting using a well counter (Ludlum model 243) at an energy peak of 140 keV. A ^{137}Cs source was used to calibrate the well counter at 662 keV and to determine the constancy. Peak validation was then performed for ^{99m}Tc (140 keV) using a ^{99m}Tc source.

The calibration procedure was as follows. A ^{137}Cs source was inserted to calibrate the well counter at a peak energy level of 662 keV. A ^{99m}Tc source was then inserted to validate the energy peak for ^{99m}Tc, which was at 140 keV. For further validation, the ^{99m}Tc energy spectrum was mapped between 80 and 200 keV by acquisition of a reading at every 5 keV using the same ^{99m}Tc source in the well counter. Afterward, the ^{99m}Tc dose was validated with a dose calibrator, and serial dilutions were made of small aliquots from the ^{99m}Tc dose, which had been measured in the dose calibrator. The serial dilution samples were counted in the well counter, and the counting efficiency for ^{99m}Tc was calculated. This counting efficiency was 83.1%, which was the value we used for biodistribution calculations. Three consecutive counting measurements were then performed on the same ^{99m}Tc sample; the counts were within 1.0%. The constancy test was repeated on day 2 using the ^{137}Cs source and the same ^{99m}Tc sample in triplicate to ensure that the counts were consistent with day 1 after decay correction, before measurement of high-counting-rate samples that were kept for decay from day 1. The samples were measured with a maximum count limit of 5,000 cps. Measuring serial diluted ^{99m}Tc samples with known radioactivity levels allowed the linear range of the counter to be up to 6,000 cps. Uptake values were corrected for decay and presented as %ID/g with means and SDs. Changes in the level of ^{99m}Tc-duramycin uptake in each tissue were also calculated as the ratio between irradiated and control animals.

Histology

According to in vivo radionuclide imaging studies, tissues that have elevated uptake of ^{99m}Tc-duramycin—thymus, bones, small intestine, and liver—were further analyzed for the presence of apoptosis using hematoxylin and eosin staining and the terminal deoxynucleotidyl transferase-mediated dUTP nick-end labeling (TUNEL) assay. Portions of fresh tissue specimens isolated for γ-counting studies were immediately fixed in 4% formaldehyde in phosphate buffer. The tissues were paraffin-embedded, and 4-μm sections were prepared. The TUNEL assay was performed following a standard staining protocol

provided by the manufacturer (Roche). The level of apoptosis was determined by counting TUNEL-positive nuclei in random microscopy fields and expressed as a percentage of total nuclei in terms of apoptotic index.

Statistics

A 2-tailed Student *t* test was used to examine the significance of differences among tissue specimens, with a *P* value smaller than 0.05 considered statistically significant.

RESULTS

Two-Dimensional Planar Imaging Studies

In control animals, intravenously injected ^{99m}Tc-duramycin cleared rapidly via the renal urinary tract, and the general background level was low throughout the body (Fig. 1A). Of particular note was the minimal background in the hepatic and abdominal regions. The low systemic background and fast clearance indicate that ^{99m}Tc-duramycin is appropriate for whole-body imaging applications. As demonstrated in Figure 1B, at 1 d after the 15-Gy total-body irradiation, the most prominent change in ^{99m}Tc-duramycin uptake was in the thymus, with a strong focal hot spot in the thoracic region. At the same time, major bones, presumably the bone marrow, had a significant signal (Fig. 1B). ^{99m}Tc-duramycin binding in the thymus declined over the next 2 d, becoming barely detectable on the third day after irradiation (Figs. 1C and 1D, respectively). In contrast, the signal from major bones remained persistent on days 2 and 3 (Figs. 1C and D, respectively), suggesting a difference in apoptotic potential or clearance kinetics. Despite significant levels of ^{99m}Tc-duramycin binding, ^{99m}Tc-MDP bone scanning, in which the radiopharmaceutical is adsorbed to the structure of hydroxyapatite in bones, did not detect any significant changes between control and irradiated animals in the acute phase. Representative images acquired at 24 h after irradiation are shown in Figure 2. This finding indicated a lack of changes in structural biomarkers at such an acute phase after irradiation. Accompanying the dynamic changes in the thymus and major bones, uptake of ^{99m}Tc-duramycin in the hepatic region started to rise between days 2 and 3 (Figs. 1C and 1D, respectively). The abdominal region also exhibited significant uptake, possibly associated with injuries to gastrointestinal components (*18*). Radioactivity uptake in the kidneys was elevated over this period, possibly reflecting a state of dehydration as a result of reduced water intake due to compromised gastrointestinal functions (*19*). Binding of ^{99m}Tc-duramycin remained at or near the background level in other major organs and tissues, such as the brain, lungs, skeletal muscles, and adipose tissues. The findings from these imaging studies indicate that changes in ^{99m}Tc-duramycin uptake in various tissues and organs after high-dose ionizing irradiation is unequivocally detectable in the acute phase on planar images using a conventional clinical γ-camera.

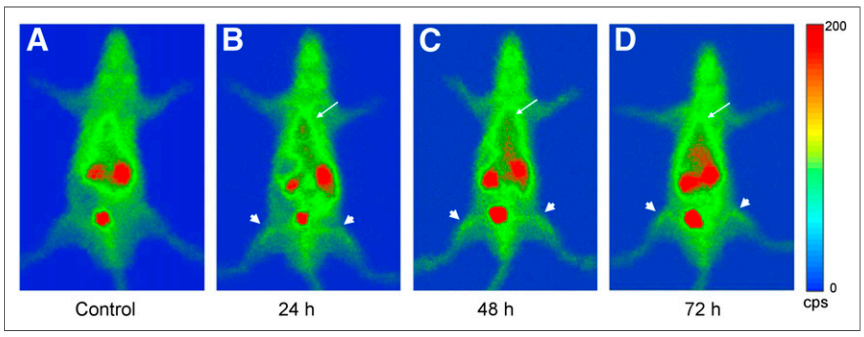

FIGURE 1. Whole-body anterior planar imaging of control (A) and 15-Gy irradiated animals at 24 h (B), 48 h (C) and 72 h (D). Focal uptake of ^{99m}Tc-duramycin in thymus is marked by arrows. Signals from major bones (femur) are marked by arrowheads.

Three-Dimensional Tomographic Imaging Studies

The early changes in ^{99m}Tc-duramycin uptake in various tissues and organs were documented using preclinical SPECT/CT in a higher spatial resolution with anatomic localization. On the basis of findings from planar imaging studies that a significant focal hot spot in the thymus was detected by 24 h after irradiation, it was decided that an earlier time point should be explored. The 3-dimensional tomographic biodistribution profile of ^{99m}Tc-duramycin in control animals was consistent with the planar imaging data (Fig. 3), in which there was a low systemic background except for the renal and urinary tract. When scanned as early as 6 h after irradiation, the thymus exhibited intense ^{99m}Tc-duramycin uptake, and in the high-resolution tomographic images the contour of the thymus was prominently delineated (Fig. 4). An elevation of signal in the gastrointestinal region was also observed (Fig. 4). On the other hand, the level of ^{99m}Tc-duramycin uptake in the bones was near that of the background (Fig. 4). At 24 h after 15 Gy of total-body irradiation, focal uptake of ^{99m}Tc-duramycin in the thymus remained distinctly visible, but the level of signal had subsided considerably compared with the 6-h time point. In the meantime, significant signals in the gut and major bones were clearly detectable on SPECT images (Fig. 5). The temporal differences in radioactivity uptake in various tissues indicated that the kinetics of programmed cell death were variable and that the apoptotic activity in the thymus is likely to reflect an early wave of cell death.

γ-Counting and Tissue Analysis

The level of ^{99m}Tc-duramycin uptake in different organs and tissues in the control, 6-h, 24-h, 48-h, and 72-h groups after 15 Gy of total-body irradiation is summarized in Figure 6 and Supplemental Table 1 (supplemental materials are available online at http://jnm.snmjournals.org). Changes in the ratios between irradiated and control tissues as a function of time are included in Supplemental Figure 1 and Supplemental Table 2. Consistent with in vivo results, radioactivity uptake in the thymus was elevated 8.5-fold at 6 h after irradiation, from 0.12 ± 0.09 to 1.02 ± 0.22 %ID/g ($P < 0.001$). The thymus signal in irradiated animals remained significantly greater than that in control animals, at 0.96 ± 0.19 ($P < 0.001$), 0.35 ± 0.11 ($P = 0.018$), and 0.53 ± 0.20 %ID/g ($P < 0.001$) at 24, 48, and 72 h after irradiation, respectively. The thymus signal was significantly lower at 48 h than at 24 h ($P = 0.0016$). This drop may have reflected the clearance of dead cells, as is consistent with thymic atrophy after irradiation. The radioactivity uptake in the thymus was not statistically significant ($P = 0.176$) between 48 and 72 h after irradiation. ^{99m}Tc-duramycin binding to the thymus correlated with high levels of apoptosis. Representative micrographs of hematoxylin- and eosin-stained and TUNEL-stained sections are shown in Figures 7A and 7D. More specifically, the apoptotic index in the thymus rose from 6.50% ± 2.61% to 61.29% ± 6.37% ($P < 0.001$) and then decreased to

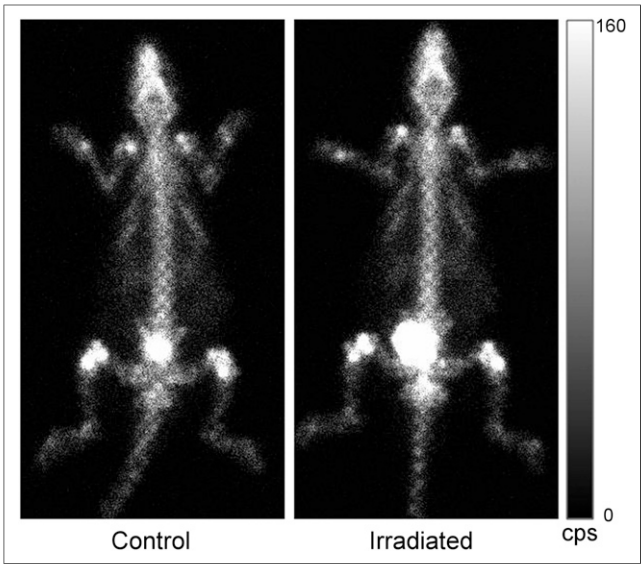

FIGURE 2. ^{99m}Tc-MDP bone scan of control animal and 15-Gy irradiated animal. No significant changes are seen at 24 h after ionizing irradiation.

41.24% ± 1.46% ($P < 0.001$), 37.92% ± 5.79% ($P < 0.001$), and 19.15% ± 1.11% ($P < 0.001$) at 24, 48, and 72 h, respectively, after irradiation. Over time, there was a decline in ^{99m}Tc-duramycin binding to the thymus and in the apoptotic index, presumably because of clearance of dead and dying cells and a reduction of accessible binding sites. This process was paralleled by thymic atrophy. At 72 h after irradiation, the tissue mass for the thymus was reduced by more than 70%, as documented by both in vivo MR imaging and dissected tissues (Supplemental Fig. 2). ^{99m}Tc-duramycin uptake in major bones was delayed, compared with that in the thymus, where it was relatively low at 6 h (0.05 ± 0.02 %ID/g, vs. control, 0.06 ± 0.03 %ID/g, $P = 0.599$) but significantly elevated at 24 h (0.11 ± 0.02 %ID/g, $P = 0.032$), 48 h (0.14 ± 0.03 %ID/g, $P < 0.001$), and 72 h (0.15 ± 0.04 %ID/g, $P = 0.011$). Compared with the transient rise in ^{99m}Tc-duramycin

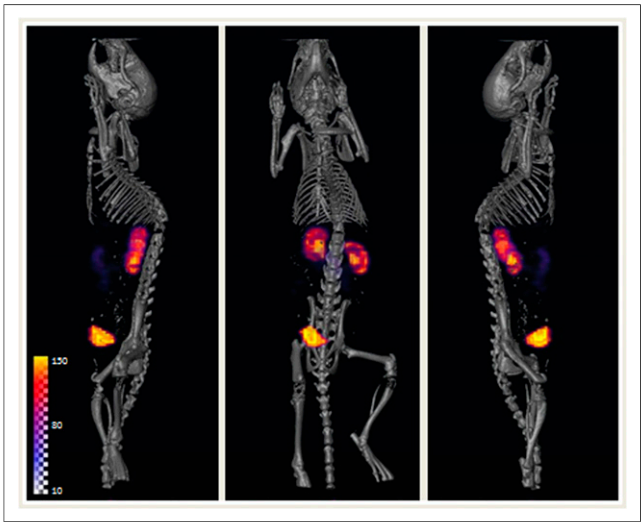

FIGURE 3. Whole-body SPECT/CT images of ^{99m}Tc-duramycin biodistribution in control animal. Renal and urinary clearance path can be seen, as well as relatively low overall background level.

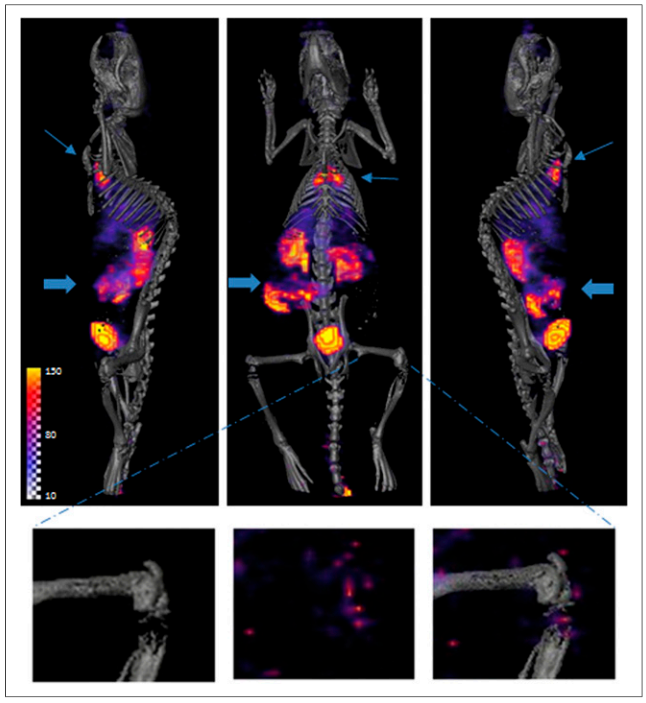

FIGURE 4. Whole-body SPECT apoptosis scan at 6 h after 15-Gy irradiation. Prominent ^{99m}Tc-duramycin uptake is detected at thymus (thin arrow) and gastrointestinal region (thick arrow). Signal from major bones (femur) was marginally detectable (insets). CT images provide anatomic coregistration. Heterogeneity in bone may reflect different degrees of mineralization.

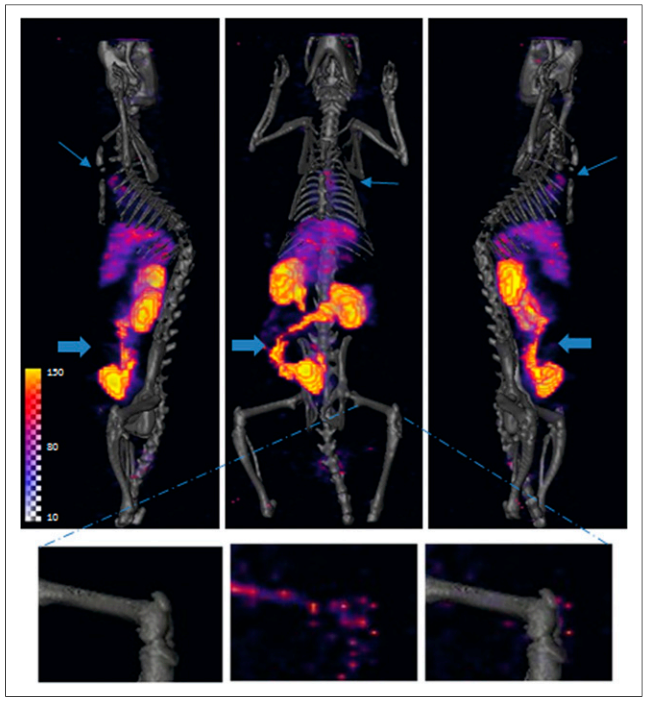

FIGURE 5. Whole-body SPECT apoptosis scan at 24 h after 15 Gy of irradiation. ^{99m}Tc-duramycin uptake is clearly detectable at thymus (thin arrow), guts (thick arrow), and major bones (femur, insets). There is also diffuse uptake in liver.

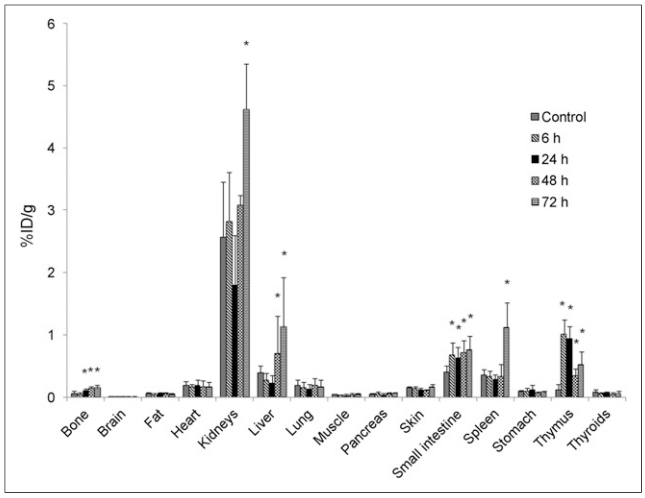

FIGURE 6. Radioactivity uptake as determined by γ-counting. Dynamics of ^{99m}Tc-duramycin uptake in different organs and tissues is described in terms of %ID/g in control animal and at 6, 24, 48 and 74 h after irradiation ($n = 4$ for each time point). Uptake values that are significantly higher ($P < 0.05$) than those of controls are highlighted with asterisks.

binding in the thymus, elevation of bone signal was more prolonged and did not show a significant decline at 72 h after irradiation. In the bone marrow, TUNEL-positive nuclei accounted for 9.76% ± 3.39% of the total number of cell nuclei in control animals and 21.05% ± 3.45% ($P = 0.003$), 45.0% ± 4.15% ($P < 0.001$), 46.55% ± 1.79% ($P < 0.001$), and 43.0% ± 5.24% ($P < 0.001$) in the 6-, 24-, 48-, and 74-h groups after irradiation (Fig. 7). An elevated level of ^{99m}Tc-duramycin uptake was detected in the gastrointestinal region at 6 h after irradiation (0.68 ± 0.19, vs. control, 0.40 ± 0.11 %ID/g, $P = 0.043$) (Fig. 4). Significantly elevated ^{99m}Tc-duramycin uptake in the small intestine was also detected at 24 h (0.64 ± 0.16 %ID/g, $P = 0.048$), 48 h (0.72 ± 0.19 %ID/g, $P = 0.027$), and 72 h (0.76 ± 0.22 %ID/g, $P = 0.026$). Regions with elevated apoptotic nuclei were found in the alimentary canal and around the crypts of the small intestine (Fig. 7). The distribution of apoptotic cells in the gut was highly heterogeneous. Once the intestines were harvested and fully extended for histologic analysis, we found it challenging to pinpoint the regions of focal uptake. It was possible that the hot-spot uptake in whole-body scans might have reflected aggregated segments from different regions of the organ. Over time after irradiation, the liver had a diffuse pattern of ^{99m}Tc-duramycin uptake. However, no significant levels of liver apoptosis were detected. The uptake was likely due to the accumulation of cellular debris or metabolic changes. The spleen also showed elevated ^{99m}Tc-duramycin binding at 72 h after irradiation. Because the focus of the current study was on the detection of early tissue injuries, the presence of apoptosis on a cellular level in the spleen was not examined by histology.

DISCUSSION

Noninvasive whole-body imaging provides a unique opportunity to look at the dynamics of tissue-dependent susceptibility to high-dose ionizing irradiation and to add to current knowledge regarding the prevalence of apoptosis in radiation-induced injuries. Being noninvasive, the imaging approach is translatable to clinical applications. As a research tool, this imaging technique will facilitate detection of radiation damage, monitoring of injury progression, and evaluation of the efficacy of therapeutic interventions.

The in vivo, whole-body apoptosis scans parallel, and are complementary to, physicochemical measurements that have been reported for the retrospective assessment of ionizing irradiation exposure. The latter mainly include dosimetric measurements using electron paramagnetic resonance and stimulated luminescence techniques (*20,21*). These methods detect radiation-induced chemical and physical changes such as the generation of radical species or photons in biologic and man-made materials. A notable advantage of these physical measurements is that the changes associated with ionizing irradiation can be quantitatively detected and that the samples can be obtained with relative ease and convenience since specimens are collected from surrounding objects and exterior tissues such as nails and hair. Comparatively, apoptosis scanning detects the presence of cell death and thus is a more direct assessment of tissue damage. As such, an apoptosis scan is likely to be useful in both external- and internal-exposure scenarios, whereas physical measurements are effective only with external exposures.

In terms of signals detected in susceptible tissues, the thymus was the earliest and the most prominent in ^{99m}Tc-duramycin uptake within hours after radiation exposure. The early peak of thymic cell death diminished by 24 h and continued to subside on days 2 and 3. These kinetics were associated with extensive thymic atrophy, whereby, in the current study, the thymic mass was reduced by more than 70% within 3 d after irradiation. The reduction of cell mass was consistent with a continued clearance of dead cells and debris, which was reflected in decreased ^{99m}Tc-duramycin binding on later days. Lymphocytes are highly sensitive to ionizing irradiation. The thymic accumulation of dead and dying circulating lym-

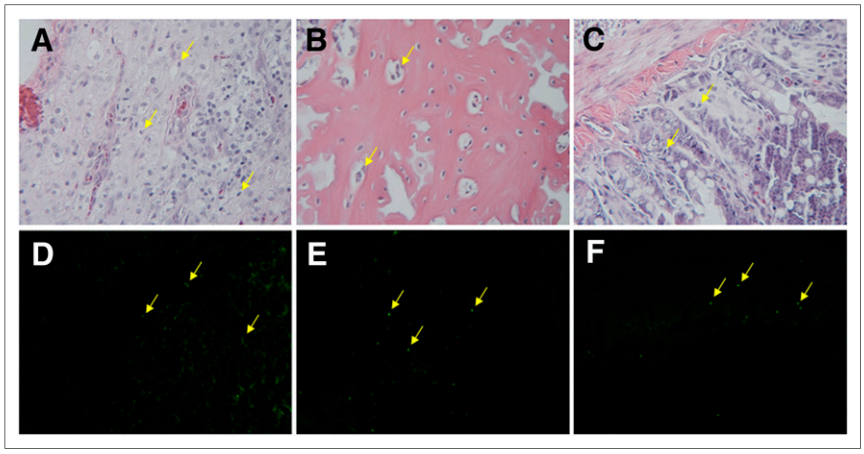

FIGURE 7. Histologic analysis. Representative hematoxylin- and eosin-stained and TUNEL-stained micrographs that demonstrate presence of apoptotic cells from tissues acquired at 24 h after irradiation are shown for thymus (A and D), femur (B and E), and small intestine (C and F). Nuclei that are characteristic of apoptosis, either fragmented, marginalized in hematoxylin and eosin, or fluorescently labeled by TUNEL, are indicated by arrows.

phocytes may also have contributed to the signal intensity. The animals enrolled in the current study were juveniles and young adults, in which the thymic mass is relatively high. It is known that the thymic mass in rats gradually decreases with age, as it does in humans. When the current findings are extrapolated to humans, focal but less intense signal may be expected from older individuals because the organ is smaller. Comparatively, the peak of thymic cell death appeared to precede signal detected from major bones, which were clearly detectable at 24 but not at 6 h. Another significant difference is that the bone signal persisted until at least 72 h after irradiation—indicative of a broader wave of cell death or a slower rate of clearance for dead cells in bones. Signal from the gut was elevated as early as 6 h after irradiation and was sustained for several days. On the basis of the current findings, the focal radioactivity uptake was indicative of tissue injuries. As such, there was a qualitative correlation between hot-spot uptake and the local density of dead and dying cells. It may be possible to determine the extent of tissue injury in a semiquantitative fashion, provided that the uptake kinetics are acquired with SPECT, with the tissue mass being measured with CT or MR imaging. The total amount of externalized PE can be derived from kinetic analysis using compartment modeling (*15*). This parameter is quantitatively related to the number of dead and dying cells. Although there are existing reports on radiation-induced cell death in other tissues, such as the central nervous system and lungs, no significant elevation of ^{99m}Tc-duramycin binding was detected in the current study, likely because of a relatively low percentage of cell death or a more diffuse distribution, which is detectable on a cellular level in histology but is below the threshold of detection of whole-body imaging. The lack of a positive readout in these tissues indicates a detection limit.

More than a decade of apoptosis imaging research has resulted in several promising agents. Among these, annexin V derivatives are by far the most widely reported and are often regarded as a reference point for gauging the incremental value of future-generation imaging agents. The legacy of annexin V–based imaging agents has constituted a significant and successful push in apoptosis imaging research. Seminal work from annexin V–based imaging studies, along with others, helped pave the way toward clinical translation by demonstrating the potential, as well as the challenges, of apoptosis imaging (*12,22–25*).

A critical level of consideration is owed to the choice of an imaging agent based on the physicochemical properties of the agent within the context of an imaging application. To this end, the in vivo imaging behaviors—namely binding kinetics and contributing factors such as blood half-life, target density, and rate of diffusion—of ^{99m}Tc-duramycin have been quantitatively studied (*15*). According to prior data, ^{99m}Tc-duramycin possesses important in vivo properties, such as low molecular weight, high binding affinity and specificity, abundant binding target, single-step radiolabeling kit formulation, stability, fast clearance, and low systemic background (*14,15,17*). Comparatively, there are several major differences between duramycin– and annexin V–based radiopharmaceuticals. First, duramycin has a lower molecular weight (2 kDa) than that of annexin V (32–36 kDa) (*26,27*). A lower molecular weight translates into a greater diffusion rate in tissue and a faster clearance. These properties lead to better target interactions and a lower background, thus contributing to a greater target-to-background ratio. Second, duramycin and annexin V bind PE and PS, respectively. Once externalized, a higher PE content provides a greater number of binding targets and thus an enhanced uptake per unit surface area in the plasma membrane (*9,11,15,28*). Third, ^{99m}Tc-duramycin has predominantly renal clearance and a minimal hepatic and gastrointestinal background level in healthy subjects (*14,15*). Thus, the radiopharmaceutical is suitable for whole-body scans. Earlier versions of ^{99m}Tc-labeled annexin V had a notable liver signal, but there has been an ongoing effort to generate derivatives with significantly reduced hepatic background and enhanced renal clearance (*29,30*). The combination of these properties indicates that ^{99m}Tc-duramycin is a qualified candidate for whole-body survey scans and has potential for clinical translation.

CONCLUSION

The current study provided a proof of concept that a whole-body scan is potentially a useful imaging tool for the detection and monitoring of tissue injuries as a result of exposure to high-dose ionizing irradiation. The temporal and spatial distribution of tissue injuries delineated using this imaging technique will contribute to a better understanding of radiation-induced tissue damage. Although further investigations are warranted, findings from this study will have broad implications in detecting externalized PE as a molecular target.

DISCLOSURE

The costs of publication of this article were defrayed in part by the payment of page charges. Therefore, and solely to indicate this fact, this article is hereby marked "advertisement" in accordance with 18 USC section 1734. This work was supported by grants 5R01HL102085 and 5U19AI067734 from the National Institutes of Health. No other potential conflict of interest relevant to this article was reported.

REFERENCES

1. Hendry JH, Potten CS, Merritt A. Apoptosis induced by high- and low-LET radiations. *Radiat Environ Biophys.* 1995;34:59–62.
2. Szumiel I. Ionizing radiation-induced cell death. *Int J Radiat Biol.* 1994;66:329–341.
3. Potten CS, Merritt A, Hickman J, Hall P, Faranda A. Characterization of radiation-induced apoptosis in the small intestine and its biological implications. *Int J Radiat Biol.* 1994;65:71–78.
4. Vincent PC. Apoptosis and the assessment of radiation injury. *Stem Cells.* 1995;13(suppl 1):153–164.
5. Held KD. Radiation-induced apoptosis and its relationship to loss of clonogenic survival. *Apoptosis.* 1997;2:265–282.
6. Harms-Ringdahl M, Nicotera P, Radford IR. Radiation induced apoptosis. *Mutat Res.* 1996;366:171–179.
7. Lavin MF. Radiation-induced cell death and its implications in human disease. *Results Probl Cell Differ.* 1998;24:213–232.
8. Daleke DL. Regulation of transbilayer plasma membrane phospholipid asymmetry. *J Lipid Res.* 2003;44:233–242.
9. Bevers EM, Comfurius P, Dekkers DW, Zwaal RF. Lipid translocation across the plasma membrane of mammalian cells. *Biochim Biophys Acta.* 1999;1439:317–330.
10. Williamson P, Schlegel RA. Transbilayer phospholipid movement and the clearance of apoptotic cells. *Biochim Biophys Acta.* 2002;1585:53–63.
11. Emoto K, Toyama-Sorimachi N, Karasuyama H, et al. Exposure of phosphatidylethanolamine on the surface of apoptotic cells. *Exp Cell Res.* 1997;232:430–434.
12. Blankenberg FG, Katsikis PD, Tait JF, et al. In vivo detection and imaging of phosphatidylserine expression during programmed cell death. *Proc Natl Acad Sci USA.* 1998;95:6349–6354.
13. Zhao M, Beauregard DA, Loizou L, Brindle KM. Non-invasive detection of apoptosis using magnetic resonance imaging and a targeted contrast agent. *Nat Med.* 2001;7:1241–1244.
14. Zhao M, Li Z, Bugenhagen S. ^{99m}Tc-labeled Duramycin as a novel phosphatidylethanolamine-binding molecular probe. *J Nucl Med.* 2008;49:1345–1352.

15. Audi S, Li Z, Capacete J, et al. Understanding the in vivo uptake kinetics of a phosphatidylethanolamine-binding agent ^{99m}Tc-Duramycin. *Nucl Med Biol.* 2012;39:821–825.
16. Edwards DS, Liu S, Barrett JA, et al. New and versatile ternary ligand system for technetium radiopharmaceuticals: water soluble phosphines and tricine as co-ligands in labeling a hydrazinonicotinamide-modified cyclic glycoprotein IIb/IIIa receptor antagonist with ^{99m}Tc. *Bioconjug Chem.* 1997;8:146–154.
17. Zhao M, Li Z. A single-step kit formulation for the ^{99m}Tc-labeling of HYNIC-Duramycin. *Nucl Med Biol.* 2012;39:1006–1011.
18. Miyoshi-Imamura T, Kakinuma S, Kaminishi M, et al. Unique characteristics of radiation-induced apoptosis in the postnatally developing small intestine and colon of mice. *Radiat Res.* 2010;173:310–318.
19. Sharma M, Sharma R, Ge XL, et al. Early detection of radiation-induced glomerular injury by albumin permeability assay. *Radiat Res.* 2001;155:474–480.
20. Trompier F, Bassinet C, Wieser A, De Angelis C, Viscomi D, Fattibene P. Radiation-induced signals analysed by EPR spectrometry applied to fortuitous dosimetry. *Ann Ist Super Sanita.* 2009;45:287–296.
21. Woda C, Bassinet C, Trompier F, Bortolin E, Della Monaca S, Fattibene P. Radiation-induced damage analysed by luminescence methods in retrospective dosimetry and emergency response. *Ann Ist Super Sanita.* 2009;45:297–306.
22. Hofstra L, Liem IH, Dumont EA, et al. Visualisation of cell death in vivo in patients with acute myocardial infarction. *Lancet.* 2000;356:209–212.
23. Lahorte CMM, VanderHeyden JL, Steinmetz N, et al. Apoptosis-detecting radioligands: current state of the art and future perspectives. *Eur J Nucl Med.* 2004; 31:887–919.
24. Narula J, Acio ER, Narula N, et al. Annexin-V imaging for noninvasive detection of cardiac allograft rejection. *Nat Med.* 2001;7:1347–1352.
25. Belhocine T, Steinmetz N, Hustinx R, et al. Increased uptake of the apoptosis-imaging agent ^{99m}Tc recombinant human Annexin V in human tumors after one course of chemotherapy as a predictor of tumor response and patient prognosis. *Clin Cancer Res.* 2002;8:2766–2774.
26. Hayashi F, Nagashima K, Terui Y, et al. The structure of PA48009: the revised structure of Duramycin. *J Antibiot (Tokyo).* 1990;43:1421–1430.
27. Huber R, Römisch J, Paques EP. The crystal and molecular structure of human annexin V, an anticoagulant protein that binds to calcium and membranes. *EMBO J.* 1990;9:3867–3874.
28. Spector AA, Yorek MA. Membrane lipid composition and cellular function. *J Lipid Res.* 1985;26:1015–1035.
29. Tait JF, Smith C, Blankenberg FG. Structural requirements for in vivo detection of cell death with ^{99m}Tc-annexin V. *J Nucl Med.* 2005;46:807–815.
30. Mukherjee A, Kothari K, Tóth G, et al. ^{99m}Tc-labeled annexin V fragments: a potential SPECT radiopharmaceutical for imaging cell death. *Nucl Med Biol.* 2006;33:635–643.